Dalton Transactions

ROYAL SOCIETY OF CHEMISTRY

PAPER

View Article Online
View Journal | View Issue

Cite this: *Dalton Trans.*, 2026, **55**, 5397

Synthesis of hybrid phosphinoferrocene ligands bearing amine pendants and catalytic evaluation of their gold(I) complexes

David Rezazgui, Ivana Císařová, Petr Štěpnička and Jiří Schulz *

A series of hybrid, ferrocene-based phosphines bearing additional amine substituents have been synthesized and evaluated in gold catalysis. The series includes 1,1′- and 1,2-disubstituted phosphinoferrocene donors with cyclic or acyclic amine groups (morpholine, thiomorpholine, and dimethylamine) and various substituents on the phosphorus atom (phenyl, cyclohexyl, and 2-furyl). The compounds were prepared using two complementary routes: (1) alkylation of a sulfide-protected phosphine–amine intermediate and (2) copper-catalyzed electrophilic amination followed by a lithiation/phosphinylation step. The corresponding chlorogold(I) complexes [AuCl(L-κ*P*)], obtained in high yields and structurally characterized, were evaluated as precatalysts in intramolecular cyclization of *N*-propargylbenzamide into 4,5-dihydro-5-methylene-2-phenyloxazole and oxidative cyclization of phenylacetylene with acetonitrile (using pyridine *N*-oxide as the oxidant) to 2-methyl-5-phenyl-1,3-oxazole. Catalytic studies revealed that the nature of the amine and phosphine substituents strongly influences the catalyst performance. Compared with their 1,2-disubstituted (homoannular) analogs, the complexes obtained from 1,1′-disubstituted (heteroannular) ligands generally exhibited faster reaction rates. In addition, a specific structural distortion of the ferrocene unit comprising the bending of the N-bound cyclopentadienyl carbon atom from the ring plane was detected in the structures of compounds bearing an amine group as the sole substituent on the cyclopentadienyl ring. This distortion was rationalized using DFT calculations as a consequence of the mesomeric effect of the amine moiety, which affects the electron distribution in the cyclopentadienyl ring.

Received 6th February 2026,
Accepted 6th March 2026

DOI: 10.1039/d6dt00321d

rsc.li/dalton

Introduction

In the past decade, gold catalysis has evolved into a useful synthetic tool.[1,2] One of the reasons for this development has been the use of purposely designed bidentate P,N-donor ligands.[3] These hybrid donors, which often combine soft phosphorus (typically phosphine) and hard nitrogen (usually amine or imine) donor groups, have become indispensable for homogeneous transition metal catalysis.[4] Their donor asymmetric, hemilabile nature and great structural variability are particularly useful for achieving control over the catalytic activity of a ligated metal center, which is unattainable with monodentate ligands.[5]

Bifunctional P,N-donors have recently been applied in gold(I) catalysis, even though gold(I) forms almost exclusively linear two-coordinated complexes and prefers soft donor atoms such as P and S.[6] For example, the use of suitably designed bidentate P,N-donors helped to overcome the reluctance of gold(I) to undergo oxidative addition.[3e] Bourissou *et al.* reported that even a simple P,N-chelating ligand could induce the oxidative addition of aryl halides to Au(I) under mild conditions.[7] The hemilabile character of the ligand was crucial because the hard nitrogen group stabilized the formed Au(III) center and lowered the reaction barrier. This approach has been successfully extended to enantioselective catalysis when a carefully designed chiral P,N-bidentate ligand that combines a bulky phosphine group with a C_2-symmetric chiral amine moiety was used.[8]

In addition to enabling new redox pathways in gold catalysis, P,N ligands can also engage in catalysis through metal–ligand cooperation.[9] Cooperation between a metal and a ligand may facilitate substrate activation or assist in chiral induction. In such cases, the nitrogen donor group does not coordinate gold(I) but enables specific interactions with a substrate molecule, typically *via* hydrogen bonding.[10] For instance, remote nitrogen-based functional groups such as amides, amines, or tertiary anilines in hybrid phosphine ligands can facilitate the addition of protic nucleophiles to alkynes and

Department of Inorganic Chemistry, Faculty of Science, Charles University, Hlavova 2030, 12800 Prague, Czech Republic. E-mail: jiri.schulz@natur.cuni.cz

allenes through ligand-assisted substrate deprotonation.[11] As already mentioned, the ability of some nitrogen donor groups to form noncovalent interactions can be used to achieve chiral induction in enantioselective gold(I) catalysis.[12]

We recently synthesized a group of ferrocene ligands[13] that combine soft phosphine and hard amine donor groups in their molecules.[14] During our work, we realized that the number of ferrocene-based P,N ligands with a nitrogen donor group attached *directly* to the ferrocene backbone is surprisingly limited, especially when considering the successful catalytic applications of P,N-ligands from the DalPhos family.[15] Therefore, we decided to synthesize a group of cognate phosphinoferrocene ligands bearing amine pendant groups (Scheme 1) and investigate whether the combination of the distinct geometric and electronic properties of the ferrocene skeleton[13] and the presence of the P- and N-donor groups is beneficial for gold catalysis.

Results and discussion

Synthesis and characterization of the ligands

First, we attempted to prepare the targeted ligands by alkylation of 1′-(diphenylphosphino)-1-aminoferrocene.[16] This starting material had to be used in a P-protected form to avoid undesired alkylation of the already "installed" phosphine group. Our initial experiments revealed that borane protection[17] was not suitable for this purpose because the reaction of 1′-(diphenylphosphino)-1-aminoferrocene–borane (1 : 1) with bis(2-chloroethyl)ether not only led to complete deprotection of the phosphine moiety but was probably accompanied by alkylation of the phosphine group without any observable formation of the desired product. Therefore, we protected the phosphine group by thionation (Scheme 2). The required 1′-(diphenylthiophosphoryl)-1-aminoferrocene (**8**) was obtained by lithiation/azidation of 1′-(diphenylthiophosphoryl)-1-bromoferrocene with 4-toluenesulfonyl azide (TsN_3) and reduction of the resulting azide by $Li[AlH_4]$ (see the SI).

Subsequent alkylation of **8** with bis(2-chloroethyl)ether produced the desired product **1aS** in good yield. The following desulfuration with RANEY® nickel in acetonitrile afforded phosphine–amine **1a** as an orange crystalline solid (N.B. The use of other solvents such as THF or MeOH resulted in partial or even complete removal of the phosphine group[18]).

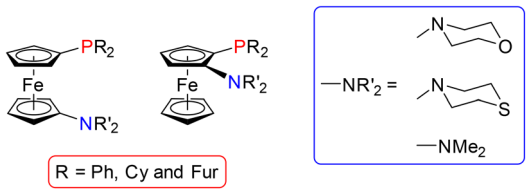

Scheme 1 General formulas of the hybrid ferrocene-based P,N-donors reported in this contribution (Cy = cyclohexyl, Fur = 2-furyl).

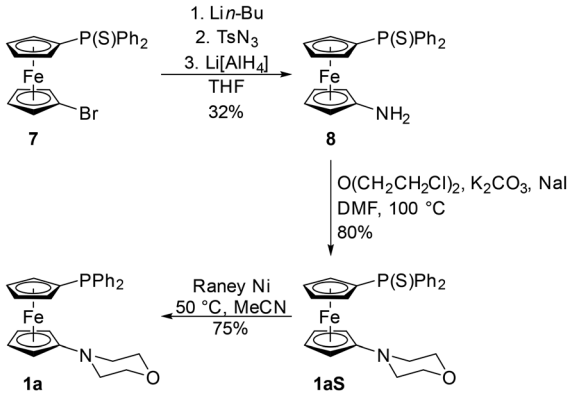

Scheme 2 Synthesis of phosphinoamine **1a** (TsN_3 = 4-toluenesulfonyl azide, DMF = *N*,*N*-dimethylformamide).

Compound **1a** and all intermediates were characterized by common spectroscopic methods (^1H, $^{13}C\{^1H\}$, and $^{31}P\{^1H\}$ NMR spectroscopy and ESI mass spectrometry) and elemental analysis. The ^1H and $^{13}C\{^1H\}$ NMR spectra of **1a** exhibited a characteristic set of signals due to the asymmetrically 1,1′-disubstituted ferrocene unit as well as the signals arising from the PPh_2 unit and the CH_2 groups of the morpholine substituent. The ESI-MS spectra displayed a peak for the pseudomolecular ion $[M + H]^+$ at m/z 456.0.

The molecular structure of **1a** is shown in Fig. 1 (for the crystal structure of **8**, see the SI). The substituents on the ferrocene unit assume an approximately 1,2′ conformation[19] with $\tau = -85.6(2)°$ (τ is the torsion angle C1–Cg1–Cg2–C6, where Cg1 and Cg2 are the centroids of the cyclopentadienyl rings C(1–5) and C(6–10), respectively), and the dihedral angle of the least-squares cyclopentadienyl planes is 5.4(1)°. A more detailed inspection of the structure, however, reveals a specific

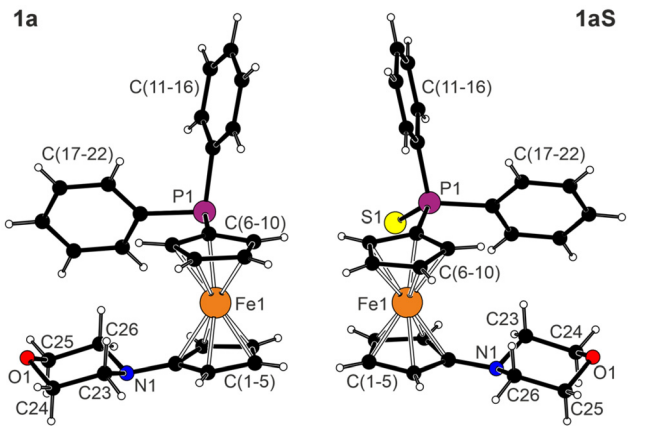

Fig. 1 Molecular structures of **1a** and **1aS**. Selected distances and angles (in Å and °), for **1a**: Fe1–C(1–10) range 2.024(2)–2.106(2), P1–C6 1.814(2), P1–C11 1.839(2), P1–C17 1.831(2), C1–N1 1.404(3); for **1aS**: Fe1–C(1–10) range 2.020(2)–2.110(2), P1–C6 1.787(2), P1–C11 1.820(2), P1–C17 1.813(2), P1–S1 1.9491(8), C1–N1 1.398(3). Displacement ellipsoid plots are available in the SI.

distortion of the ferrocene unit comprising bending of the pivotal atom C1 (the varying Fe–C distances are already hinting in that direction). In particular, atoms C(2–5) constitute a virtually ideal plane from which the C1 atom is displaced by 0.045(2) Å in the direction away from the iron atom. In contrast, the carbon atoms in the cyclopentadienyl ring C(6–10) are coplanar within ≈0.003 Å.

The phosphine group in **1a** has a geometry similar to that in (diphenylphosphino)ferrocene ($FcPPh_2$, Fc = ferrocenyl).[20] One phenyl substituent is directed above the ferrocene unit, and the other is directed to the side. The lone pair thus occupies a space on the side of the ferrocene unit and is directed away from the morpholinyl group, which has a chair conformation and geometry similar to that in 4-ferrocenylmorpholine (*vide infra*).

Notably, similar deformation at the ferrocene unit is observed in the molecule of **1aS** (Fig. 1), which is otherwise similar to the structure of free phosphine **1a**, including the molecular conformation (τ = 82.1(2)°). As expected, a difference is seen at the phosphorus substituent, which exhibits shorter P–C bonds and wider C–P–C angles. These parameters, as well as the P1–S1 distance (1.9491(8) Å), are unexceptional considering the data for $FcP(S)Ph_2$ (1.9363(8) Å at room temperature).[21]

Although the synthesis of ligand **1a** using the described method was successful, it involved too many reaction steps. Therefore, we sought an alternative approach that would be more straightforward and would allow an easier modification of the functional substituents. We envisaged that this reaction sequence could involve catalytic amination of 1,1′-dibromoferrocene followed by phosphinylation, yielding the desired P,N-ligands in only two steps. Unfortunately, our initial attempts using Ullman coupling[22] and Buchwald–Hartwig[23] amination failed. Hence, we resorted to copper-catalyzed electrophilic amination of arylzinc intermediates. Reactions of this kind have emerged as a versatile tool in organic and organometallic synthesis, offering a straightforward route to the generation of C–N bonds.[24] They usually involve the coupling of nucleophilic organometallic reagents with electrophilic nitrogen sources, such as *O*-benzoyl hydroxylamine derivatives and *N*-chloroamines, mediated by transition metal catalysts. For instance, Johnson *et al.* reported that copper-catalyzed electrophilic amination with arylzinc reagents offers high functional group tolerance and mild reaction conditions.[25] Inspired by this approach, we examined the reaction of the *in situ*-generated ferrocenylzinc bromide with *O*-benzoyl-*N*-hydroxymorpholine catalyzed by copper(II) chloride (Scheme 3).

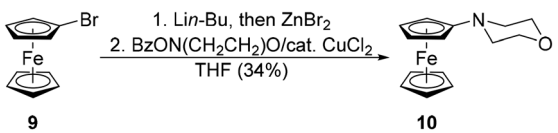

9 10

Scheme 3 Synthesis of 4-ferrocenylmorpholine (**10**; Bz = benzoyl).

To our delight, the reaction produced 4-ferrocenylmorpholine (**10**) in moderate yield (34% after recrystallization; for the crystal structure of **10**, see the SI), albeit only when 2 equiv. of lithioferrocene (and FcZnLi) *per* equivalent of *O*-benzoyl-*N*-hydroxymorpholine were used. This stoichiometry occurs possibly because the active species undergoing amination is bis(ferrocenyl)zinc, which can deliver only one ferrocenyl group during the reaction. Attempts to overcome this limitation by varying the stoichiometry of the reactants and the copper catalysts (*e.g.*, copper(I) triflate) were unsuccessful.

In the next step, we tested whether this procedure could be applied for the electrophilic amination of 1,1′-dibromoferrocene (**11**). Indeed, (1′-bromoferrocenyl)zinc bromide generated *in situ* was smoothly converted to 1-bromo-1′-(morpholin-4-yl) ferrocene (**12a**; Scheme 4) *via* reaction with *O*-benzoyl-*N*-hydroxymorpholine mediated by copper(II) chloride. This compound was subsequently phosphinylated using the standard lithiation/phosphinylation protocol[26] to produce compound **1a** in two steps from the commercially available **11**. The isolated yield over the two steps was 41%.

The scope of the reaction was demonstrated by the synthesis of 1,1′-disubstituted phosphinoamines **1a–c**, **2a**, and **3a**, which differ in the amine part or by substituents on the phosphorus atom (Scheme 4, Route A), as well as by the preparation of their planar-chiral, 1,2-disubstituted isomers (compounds **4a–c**, **5a**, and **6a**) from bromoferrocene **9**, employing *ortho*-directed lithiation of this substrate[27] during the first step (Scheme 4, Route B). In this manner, we synthesized the full range of ligands bearing the diphenylphosphinyl group, and for ligands with the morpholinyl pendant group, we also obtained compounds differing at the phosphine moiety to produce ligands featuring more (R = Cy; **2a** and **5a**) and less (R = Fur; **3a** and **6a**) electron-donating phosphine groups.

Phosphinoamines **1–6** were authenticated by NMR spectroscopy, mass spectrometry, and elemental analysis. We note

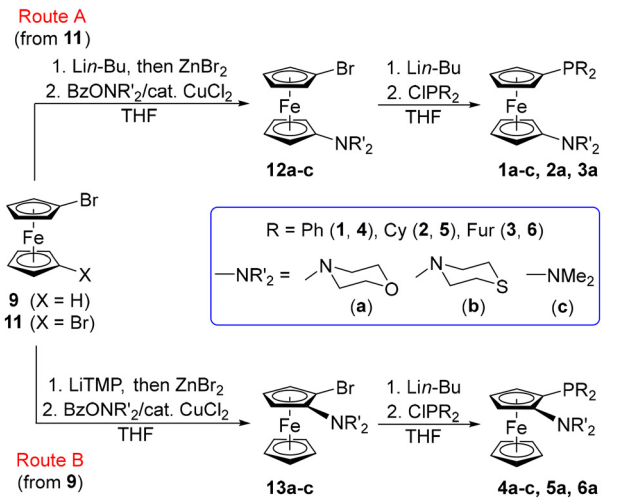

Scheme 4 Synthesis of phosphine–amines **1a–c**, **2a**, **3a** and **4a–c**, **5a**, and **6a** (Cy = cyclohexyl, Fur = 2-furyl, Bz = benzoyl; LiTMP = lithium 2,2,6,6-tetramethylpiperidide).

that compounds **1c** [28] and **4c** [29] have already been described in the literature. The ^{1}H and $^{13}C\{^{1}H\}$ NMR spectra of heteroannular derivatives **1a–c**, **2a**, and **3a** displayed the expected signals, namely, four signals due to the ferrocene CH groups (which were accompanied by two additional signals of the ferrocene C^{ipso} carbons in the $^{13}C\{^{1}H\}$ NMR spectra), and resonances arising from the amine pendants (two multiplets due to CH_2 groups of morpholine or thiomorpholine moieties and a singlet of the NMe_2 group) and the PR_2 groups. For the homoannular derivatives **4a–c**, **5a**, and **6a**, the patterns changed as expected. In the ^{1}H and $^{13}C\{^{1}H\}$ NMR spectra, the ferrocene-1,2-diyl moiety gave rise to a sharp singlet due to the unsubstituted cyclopentadienyl ring and three multiplets of the CH groups on the substituted ring. In addition, the $^{13}C\{^{1}H\}$ NMR spectra revealed additional signals attributable to the ferrocene C^{ipso} carbons. Because these substances are planar chiral, some carbon atoms became diastereotopic and anisochronic. This situation was reflected by the doubling of the number of $^{13}C\{^{1}H\}$ NMR signals due to the (thio)morpholine NCH_2 groups and substituents on the phosphine moieties (PR_2). The $^{31}P\{^{1}H\}$ NMR signals were observed within the usual ranges.[30]

In addition to the spectroscopic characterization, the crystal structures of **1b**, **1c**, **2a**, **3a**, **4a**, **4b**, **4c**, **5a**, and **6a** were determined by single-crystal X-ray diffraction analysis (the structure of **1a** was discussed earlier). The structures are generally similar and, hence, only selected structures and structural aspects are presented here. The complete data and displacement ellipsoid plots are available in the SI.

The molecules of **1b**, **1c** (Fig. 2), **2a**, and **3a** share an overall arrangement with **1a**. One phosphine substituent on the ψ-tetrahedral phosphorus atom is directed above the ferrocene unit, and the other is directed toward or away from the amine moiety. Like **1a**, the ferrocene unit in the structures shows structural deformation involving displacement of the N-bound cyclopentadienyl ring carbon atom (C1) away from the iron center. However, this distortion is somewhat smaller than that in **1a**. The substituents appended in positions 1 and 1′ of the ferrocene unit in **1c** (τ = −78.34(9)°) are oriented similarly to those in **1a** (*i.e.*, they adopt an approximately 1,2′ conformation), while those in the other compounds are more distant, as indicated by the τ angles of −147.9(2)° for **1b**, 148.0(1)° for **2a**, and −111.35(8)° for **3a**. The amine substituents exhibit the expected arrangement, including the chair conformation of the (thio)morpholinyl groups.

The 1,2-isomeric compounds **4a** (Fig. 3), **4b**, **5a**, and **6a** are planar-chiral but racemic and crystallize with the symmetry of the centric space groups or as a racemic twin (only **4b**). Notably, the proximal pnictine substituents in these structures impose no significant torsion on the cyclopentadienyl ring, as evidenced by the N1–C1–C2–P1 angles below 8°, and the ferrocene unit does not exhibit the characteristic structural distortion, at least not in a similar extent (for instance, the Fe1–C1 bonds in **4a** and **4c** are still the longest among the Fe1–C(1–5) bonds). The phosphine substituents are oriented similarly to those in the 1,1′-isomeric compounds, with their lone pair directed toward the nitrogen pendants.

The peculiar distortion of the ferrocene unit, detected in the structures of ferrocene amines and their 1′-phosphinylated derivatives, was also found when the structural data of aminoferrocene[31] were revisited. Notably, a similar structural deformation, but in the *opposite* sense (*i.e.*, a shortening of the Fe–C^{ipso} distance and inclination of the substituent to the Fe atom) was previously observed for (dibromoboryl)ferrocene.[32] In turn, this suggested a systematic influence and led us to examine this structural phenomenon in detail using DFT calculations and 4-ferrocenylmorpholine (**10**) as the model compound.

The calculations revealed that the elongation of the Fe1–C1 bond in the structure of **10** reflects the electronic polarization of the substituted cyclopentadienyl ring C(1–5) induced by the amine substituent. IBO analysis[33,34] indicated partial delocalization of the nitrogen lone pair (lp) into the π-system of this cyclopentadienyl ring (Fig. 4), which perturbs the π-electron distribution and leads to asymmetric Fe–ring interactions, manifested by a longer Fe1–C1 bond. This interpretation was supported by topological analysis of the electron density (QTAIM). For the C(1–5) ring, the lowest electron density at the Fe–C bond critical point (bcp) was observed for the Fe1–C1

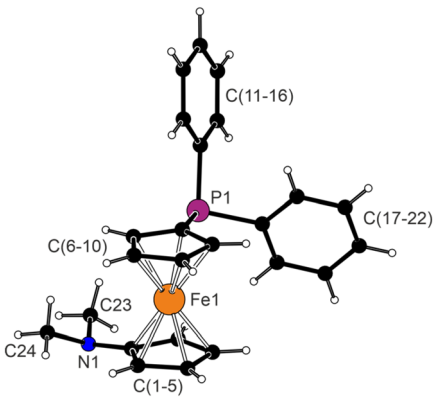

Fig. 2 Molecular structure of **1c**.

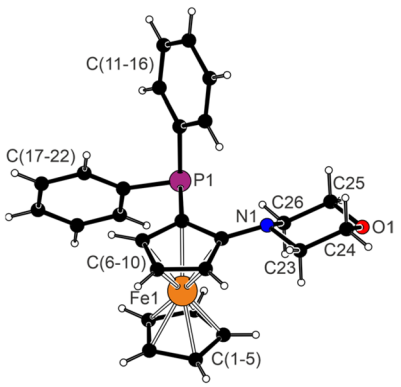

Fig. 3 Molecular structure of **4a**. Only one orientation of the disordered benzene ring C(17–22) is shown for clarity.

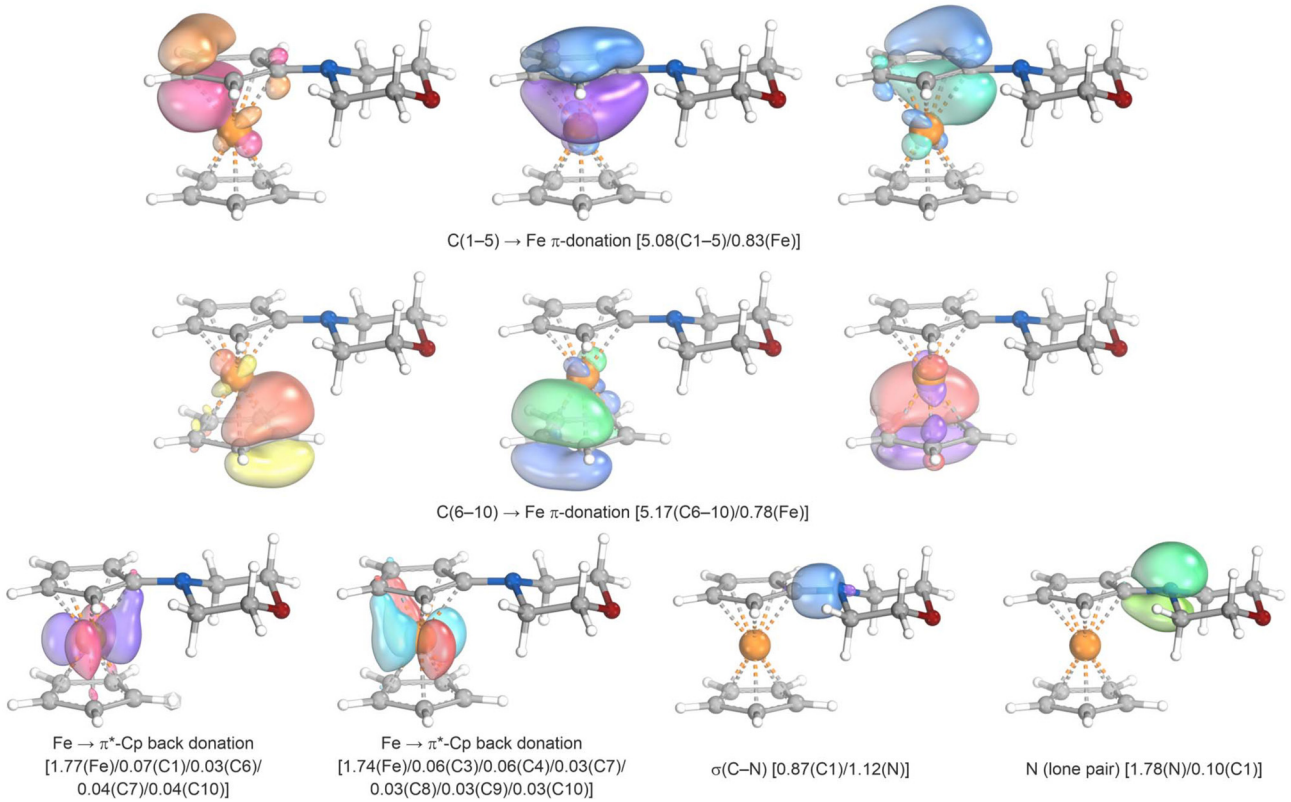

Fig. 4 Selected intrinsic bond orbitals (IBOs) representing Fe–Cp (Cp = cyclopentadienyl) bonding in **10**. Values in parentheses indicate IBO electron populations assigned to the indicated atoms or fragments.

bond (Table S8). Additional QTAIM descriptors evaluated at the bcp (*e.g.*, *H* at the bcp) together with the Mayer bond orders[35] consistently indicated a weaker Fe1–C1 interaction than the remaining Fe1–C(2–5) bonds. The IBO populations (Fig. 4) further suggested that the C(1–5) ring in **10** acts as a slightly better donor for iron than the unsubstituted ring C(6–10) {π(C(1–5)) → Fe [5.08(∑C1–C5)/0.83(Fe)]} *vs.* {π(C(6–10)) → Fe [5.17(∑C6–C10)/0.78(Fe)]}, whereas the unsubstituted ring is a better acceptor in the Fe → cyclopentadienyl back-donation {e_2(Fe) → π*(C(6–10)): [3.50(Fe)/0.24 (C6–10)] *vs.* e_2(Fe) → π*(C(1–5)): [3.50(Fe)/0.19(C1–C5)]}. Here, a larger Fe population in the π(cyclopentadienyl) → Fe IBO is considered an indication of greater donation. Conversely, the larger population of carbon atoms in both d(Fe) → π*(cyclopentadienyl) IBOs suggests stronger back-donation.

Calculations performed for the isomeric compounds **1a** and **4a** were also consistent with the experimental data (see the SI). In **1a**, the influence of the substituents can be regarded as rather independent, although they still affect the π-donation and π-back donation interactions between the cyclopentadienyl rings and Fe. The strongly electron-donating amine group with suitably positioned lone pair is conjugated with the cyclopentadienyl ring and affects its geometry similarly to **10**. Conversely, the diphenylphosphino group shows a modest overall electron-withdrawing ability, and its lone pair mixes much less efficiently with the cyclopentadienyl ring orbitals. As such, it has only a minor structural influence. For the isomeric compound **4a**, the influence of the two pnictogen substituents seems to partly compensate.

To test whether the suppression of N(lp) → C(1–5) π-donation decreases the binding asymmetry, we also studied the *N*-methylated derivative **(10Me)[BF_4]** (Scheme 5). Quaternization of the nitrogen eliminates the neutral amine lone pair as a potential π-donor. Accordingly, the crystal structure of **(10Me)[BF_4]** lacks the typical structural distortion and reveals that the Fe1–C1 distance is substantially shorter than that in **10** (*vide infra*). This structural change is again consistent with the electronic structure descriptors obtained from the IBO and QTAIM analyses (see Fig. S16 and Table S9 in the SI). In particular, IBO populations indicate that the ring C(1–5) becomes a weaker donor to Fe than the unsubstituted ring C(6–10) {π(C(1–5)) → Fe: [5.19(C1–C5)/0.73(Fe)] *vs.* π(C(6–10)) → Fe: [5.04

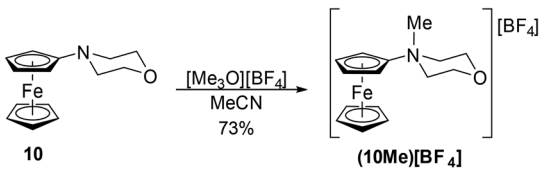

10 (10Me)[BF_4]

Scheme 5 Alkylation of **10** with Meerwein salt to give ammonium salt **(10Me)[BF_4]**.

(C6–C10)/0.91(Fe)]} and, conversely, a better acceptor for the back-donation {e_2(Fe) → π*(C(1–5)): [3.49(Fe)/0.24(C1–C5)] *vs.* e_2(Fe) → π*(C(6–10)): [3.49(Fe)/0.16(C6–C10)]}. Thus, the reversed trend in the Fe–C distances correlates with a redistribution of the π-electron density within the substituted cyclopentadienyl ring (*cf.* the π-electron populations at C1: 0.87 in **10** and 1.16 in **(10Me)[BF$_4$]**), which is consistent with the electronic polarization induced by the nitrogen substituents. Notably, the above analyses were performed on DFT-optimized geometries starting from the experimental X-ray structures. Nevertheless, the observed features remained unchanged when single-point calculations and experimental X-ray geometries were used.

The molecular structures of **10** and **(10Me)[BF$_4$]** match the results of the theoretical analysis (Fig. 5). The ferrocene unit in **10** exhibits the mentioned structural distortion (Fe–C: 2.036(1)–2.088(1) Å), with the C1 atom displaced by 0.032(1) Å from the plane defined by the remaining ring atoms C(2–5). No such distortion is detected in the structure of **(10Me)[BF$_4$]** (Fe–C: 2.005(2)–2.056(3) Å), where the Fe1–C1 distance is even the shortest. As shown in Tables S8 and S9, the experimental Fe–C distances are very well reproduced by DFT calculations.

The morpholinyl groups in both structures adopt chair conformations with a puckering parameter θ [36] near the ideal value of 0/180° (θ = 4.3(1)° and 4.4(2)° for **10** and **(10Me)[BF$_4$]**, respectively). However, while the morpholine pendant in **10** is practically parallel to the bonding cyclopentadienyl ring, in **(10Me)[BF$_4$]**, these two fragments are mutually rotated. This geometry can be explained by the loss of conjugation between the nitrogen 2p electron pair and the aromatic cyclopentadienyl ring, as further indicated by the elongation of the pivotal C1–N1 bond from 1.409(2) Å in **10** to 1.477(3) Å in **(10Me)[BF$_4$]**. Despite these differences, the departure of the nitrogen atom N1 from the least-squares plane C(2–5) for **10** (0.141(1) Å), and from the C(1–5) plane in **(10Me)[BF$_4$]** (0.142(2) Å) are practically the same and can thus be attributed to steric factors.

Synthesis and characterization of gold complexes

Phosphinoamines were used to prepare a series of gold(I) phosphine complexes **1Au–6Au** (Scheme 6) by displacement of the dimethylsulfide ligand from [AuCl(SMe$_2$)]. The resulting complexes were typically isolated by precipitation and obtained as air-stable yellow solids in essentially quantitative yields. The coordination of the phosphine group clearly manifested in the ^{31}P{^{1}H} NMR spectra through a characteristic downfield shift, whereas the ^{1}H and ^{13}C NMR spectra displayed all the expected signals due to the P-bound ligand.

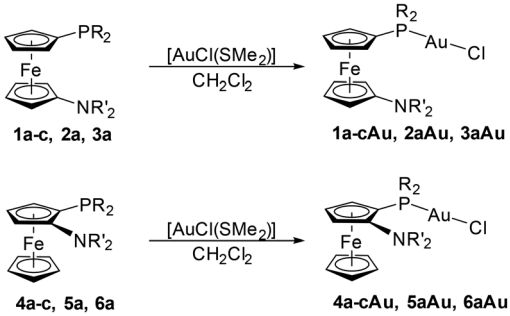

Scheme 6 Preparation of gold(I) complexes.

Crystals suitable for structural determination were obtained for all the prepared Au(I) complexes except for **6aAu** (some compounds crystallized in a solvated form). Only the molecular structures of the representative compounds **1aAu** and **4aAu** are shown in Fig. 6; structure diagrams for the remaining compounds and selected structural data are presented in the SI.

The structures consistently comprise linear P–Au–Cl units (angles: 174–179°) and exhibit Au–donor distances falling within the normal ranges.[37] The coordination of the AuCl unit results in widening of the C–P–C angles and shortening of the

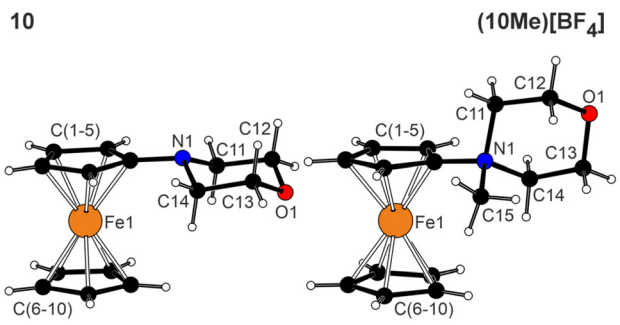

Fig. 5 Structural diagrams of **10** and the cation in the structure of the corresponding ammonium salt **(10Me)[BF$_4$]**.

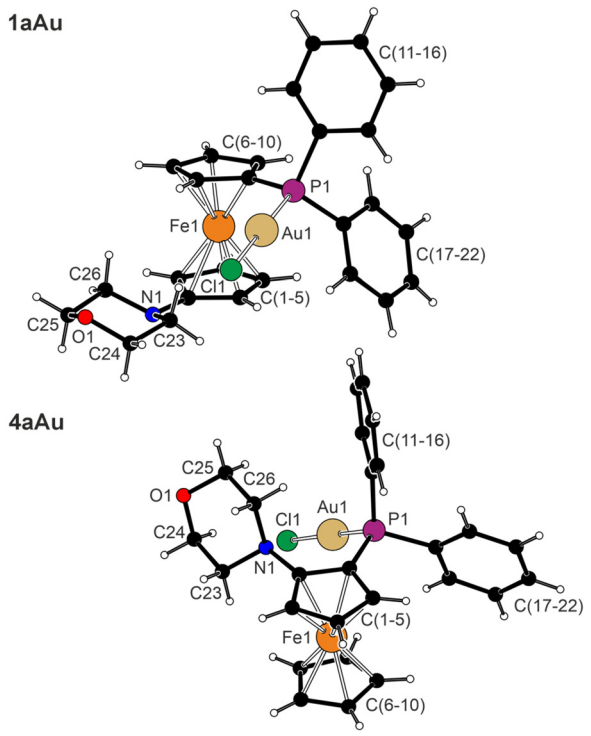

Fig. 6 Molecular structures of **1aAu** and **4aAu**. For clarity, only one orientation of the disordered ring C(11–16) is displayed.

P–C bonds relative to the respective free ligands; a similar trend is found in the $FcPPh_2$/[AuCl($FcPPh_2$-κ*P*)] pair.[20,38] The P–Au–Cl arms in all the structures are directed toward the ferrocene unit. For complexes featuring homoannular phosphinoamines, this arrangement brings the Au(I) center near the adjacent nitrogen atom with the Au–N distance below the sum of the van der Waals radii. An analysis of possible Au–N interactions in complex **4cAu** (as the model compound) by DFT calculations revealed that a so-called secondary interaction[39] is more likely than a classic, albeit weak, donor–acceptor bond. Noncovalent interactions of this kind usually arise from the presence of an electron-deficient region on the metal (σ-hole), which can attract lone-pair donors. The resulting metal–donor distances are typically shorter than the sum of van der Waals radii, as observed in this case (see the SI for details).

Notably, the ferrocene units in **1a–cAu**, **2aAu**, and **3aAu** exhibit characteristic distortion involving the displacement of pivotal C1 from the plane of the remaining cyclopentadienyl ring carbon atoms, similar to free ligands. No analogous distortion (not at least one to a similar extent) is detected for the isomeric complexes obtained from the 1,2-isomeric ligands, which maintain their regular geometry without torsion at the C1–C2 bond (N1–C1–C2–P1 < 6°).

Catalytic activity of the gold(I) complexes

The gold(I) complexes were tested as precatalysts in selected gold-catalyzed reactions. First, we chose the cyclization of *N*-propargylbenzamide (**14**) into 4,5-dihydro-5-methylene-2-phenyloxazole (**15**) (Scheme 7),[40] a simple reaction allowing *in situ* monitoring by NMR spectroscopy. Protodeauration has been suggested as the rate-limiting step for this transformation, and we thus wondered whether the phosphinoamine ligands could affect the reaction rates because of the available basic amine groups. The experiments were conducted in CD_2Cl_2 at 25 °C using 1 mol% gold complexes activated *in situ* with silver(I) bis(trifluoromethanesulfonyl)imide ($AgNTf_2$), and the progress of the reaction was followed by ^1H NMR spectroscopy. $AgNTf_2$ itself did not catalyze the reaction.

Initially, the focus was solely on comparing complexes derived from the ligands bearing the PPh_2 group. These complexes produced the desired cyclization product, usually with complete conversion under the applied reaction conditions. However, the reaction rates varied depending on the coordinated ligand. A comparison of the kinetic profiles (Fig. 7) revealed that amine groups indeed influence the catalytic reaction, with differences between complexes bearing heteroannular (**1a–c**) and homoannular (**4a–c**) ditopic ligands. Among the

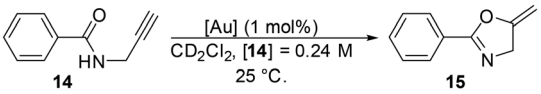

14 15

Scheme 7 Au-catalyzed cyclization of *N*-propargylbenzamide (**14**) into 4,5-dihydro-5-methylene-2-phenyloxazole (**15**).

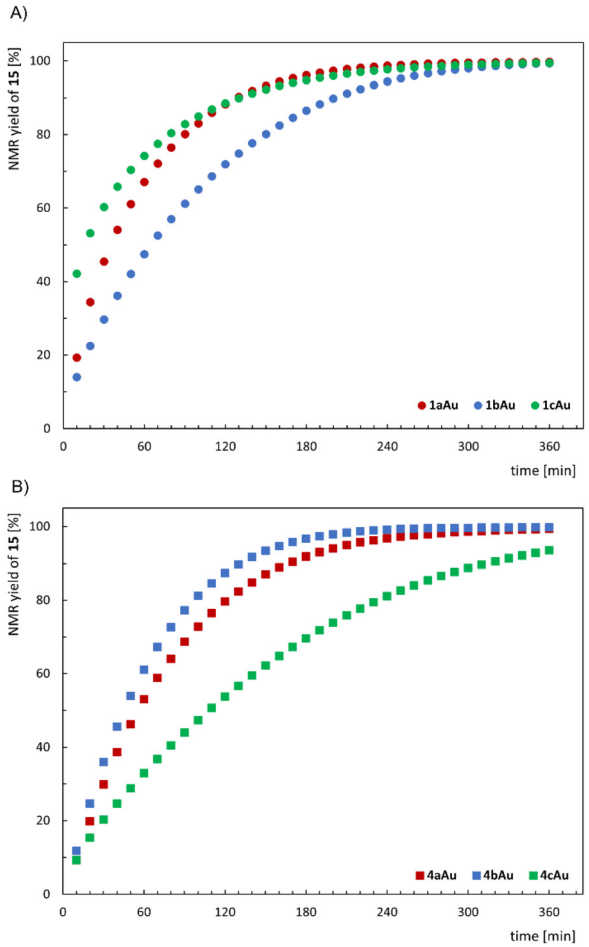

Fig. 7 Kinetic profiles for the Au-catalyzed cyclization of *N*-propargylbenzamide (**14**). The reaction was performed at 25 °C in CD_2Cl_2 in the presence of 1 mol% Au catalyst; the data are reported as the average of two independent runs. The kinetic profiles for complexes with heteroannular (A) and homoannular (B) phosphinoamine ligands are presented separately.

heteroannular derivatives, complex **1cAu**, bearing the NMe_2 group on the other cyclopentadienyl ring, was the most efficient, whereas the analogous complex **4cAu** featuring the isomeric homoannular ligand was the least active in the series of planar-chiral compounds and did not achieve complete conversion even after 6 h, unlike the other PPh_2 complexes. The catalytic activity of **1cAu** matched that of the related phosphine complex [AuCl($FcPPh_2$-κ*P*)].[41] In contrast, complex **1bAu**, which bears a thiomorpholine group, was the least active among the heteroannular derivatives, while its isomeric complex **4bAu** was the most active of the homoannular complexes. It can also be noted that generally faster reaction rates were observed for complexes with heteroannular phosphinoamine ligands.

Electron-rich phosphine ligands accelerate the cyclization reaction.[42,43] Therefore, we investigated how complexes with cyclohexyl (**2aAu** and **5aAu**) and 2-furyl (**3aAu** and **6aAu**) substituents compare with their phenyl counterparts. Surprisingly,

both of these compound families proved to be less active, although probably for different reasons. Complexes with 2-furyl substituents were inactive under the applied reaction conditions and showed activity only when 1.5 equiv. of $AgNTf_2$ was used to activate them (see Fig. S1 in the SI). This observation can be explained by the slower activation of the catalyst due to the lower *trans* effect of the weakly electron-donating $PFur_2$ ligand.[44] Interestingly, an excess of silver salt was also required to activate **5aAu** obtained from the homoannular dicyclohexylphosphine ligand, while no similar effect was observed for its heteroannular isomer **2aAu**. This comparison suggests that activation of the gold precatalyst could be inhibited or slowed down if the amine group is located in the *ortho* position relative to the phosphine moiety. A possible explanation is the formation of transient heteronuclear Au/Ag complexes.[45]

The second model catalytic reaction involved the oxidative cyclization of phenylacetylene with acetonitrile, yielding 1,3-oxazoles.[46,47] It has been suggested that an amine group in a suitably designed P,N-donor ligand may contribute to the stabilization of highly reactive α-oxo carbene intermediates in this reaction, which is necessary for their efficient trapping by an external nucleophile.[48]

The test reactions were performed using 5 mol% of gold(I) precatalyst (Scheme 8), which was again activated with a stoichiometric amount of $AgNTf_2$. The yield of the cyclization product was determined using ^{1}H NMR spectroscopy.

For this reaction, we limited the catalytic experiments to complexes with ligands bearing the PPh_2 group. Although the reactions afforded the desired product in each case, the yields were rather low and worse than the yield obtained with the reference complex [AuCl(FcPPh$_2$-κ*P*)] (Table 1). The reactions with the ligand and silver salt alone did not proceed at all. The best results were achieved with complex **1aAu**, but they were not close to the yield obtained with the model catalyst, showing that the introduced amine substituents exhibit a detrimental effect on the outcome of this particular catalytic transformation.

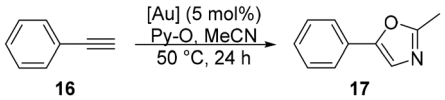

16 17

Scheme 8 Gold-catalyzed oxidative cyclization of phenylacetylene (**16**) with acetonitrile to give 1,3-oxazole **17** using pyridine-*N*-oxide (Py–O) as an oxidant.

Table 1 Gold-catalyzed oxidative cyclization of phenylacetylene **16** with acetonitrile[a]

Entry	Catalyst	Yield of **17** [%]
1	[AuCl(FcPPh$_2$-κ*P*)]	49
2	**1aAu**	18
3	**1bAu**	13
4	**1cAu**	8
5	**4aAu**	12
6	**4bAu**	13
7	**4cAu**	9

[a] Conditions: substrate **16** (0.25 mmol) and pyridine *N*-oxide (0.325 mmol, 1.3 equiv.) were reacted in acetonitrile (2.5 mL) in the presence of a gold(I) precatalyst (5 mol% Au) and silver(I) bis(trifluoromethanesulfonyl)imide (5 mol% Ag) at 60 °C for 24 h. The yields were determined by integration of the ^{1}H NMR spectra using anisole as an internal standard and represent the average of two independent runs.

Conclusions

In this study, we developed a versatile and reliable synthetic route toward P,N-hybrid phosphinoferrocene ligands involving the Cu-mediated coupling of *in situ*-generated ferrocenylzinc intermediates with benzoyloxyamines as electrophilic amination agents and subsequent lithiation/phosphinylation of bromoferrocene synthons. This method was successfully applied to prepare flexible achiral phosphinoamines containing a 1,1′-disubstituted ferrocene unit as the central scaffold and their 1,2-disubstituted, planar-chiral analogs. These phosphinoamines were used to prepare Au(I) complexes of the [AuCl(L-κ*P*)] type, which were evaluated as precatalysts in the gold-mediated cyclization of *N*-propargylbenzamide into 4,5-dihydro-5-methylene-2-phenyloxazole and in the oxidative cyclization of phenylacetylene with acetonitrile and pyridine-*N*-oxide, yielding 2-methyl-5-phenyl-1,3-oxazole. The auxiliary amine substituents at the ferrocene unit influenced the course of both catalytic transformations.

In addition, we identified a specific structural distortion in the molecules of aminoferrocene derivatives, which involves tilting the amine-substituted carbon atom away from the iron center. This distortion has been theoretically studied using DFT calculations and explained by the mesomeric effect of the amine substituent, which results in polarization of the electron density at the amine-substituted cyclopentadienyl ring.

Conflicts of interest

There are no conflicts to declare.

Data availability

The data supporting this article have been included as part of the supplementary information (SI). Supplementary information: complete experimental details, crystallographic data, structural diagrams, additional results from the DFT calculations including cartesian coordinates of the DFT optimized structures, and copies of the NMR spectra. See DOI: https://doi.org/10.1039/d6dt00321d.

CCDC 2517190–2517210, 2517404 and 2522540 contain the supplementary crystallographic data for this paper.[49a–w]

Acknowledgements

This work was supported by the Charles University Research Center program (project UNCE/24/SCI/010). Computational resources were provided by the e-INFRA CZ project (ID: 90254), supported by the Ministry of Education, Youth and Sports of the Czech Republic.

References

1 A. Fürstner and P. Davies, *Angew. Chem., Int. Ed.*, 2007, **46**, 3410–3449.
2 Recent reviews on homogeneous gold catalysis: (*a*) Z. Lu, T. Li, S. R. Mudshinge, B. Xu and G. B. Hammond, *Chem. Rev.*, 2021, **121**, 8452–8477; (*b*) C. C. Chintawar, A. K. Yadav, A. Kumar, S. P. Sancheti and N. T. Patil, *Chem. Rev.*, 2021, **121**, 8478–8558; (*c*) A. Collado, D. J. Nelson and S. P. Nolan, *Chem. Rev.*, 2021, **121**, 8559–8612; (*d*) M. Mato, A. Franchino, C. García-Morales and A. M. Echavarren, *Chem. Rev.*, 2021, **121**, 8613–8684; (*e*) D. Campeau, D. F. León Rayo, A. Mansour, K. Muratov and F. Gagosz, *Chem. Rev.*, 2021, **121**, 8756–8867; (*f*) T. Wang and A. S. K. Hashmi, *Chem. Rev.*, 2021, **121**, 8948–8978; (*g*) C. M. Hendrich, K. Sekine, T. Koshikawa, K. Tanaka and A. S. K. Hashmi, *Chem. Rev.*, 2021, **121**, 9113–9163.
3 (*a*) B. Huang, M. Hu and F. D. Toste, *Trends Chem.*, 2020, **2**, 707–720; (*b*) V. W. Bhoyare, A. G. Tathe, A. Das, C. C. Chintawar and N. T. Patil, *Chem. Soc. Rev.*, 2021, **50**, 10422–10450; (*c*) P. Font and X. Ribas, *Eur. J. Inorg. Chem.*, 2021, 2556–2569; (*d*) S. B. Ambegave and N. T. Patil, *Synlett*, 2023, 698–708; (*e*) P. Font, H. Valdés and X. Ribas, *Angew. Chem., Int. Ed.*, 2024, **63**, e202405824.
4 (*a*) S. Maggini, *Coord. Chem. Rev.*, 2009, **253**, 1793–1832; (*b*) W.-H. Zhang, S. W. Chien and T. S. A. Hor, *Coord. Chem. Rev.*, 2011, **255**, 1991–2024; (*c*) M. P. Carroll and P. J. Guiry, *Chem. Soc. Rev.*, 2014, **43**, 819–833; (*d*) P. Braunstein and A. A. Danopoulos, *Chem. Rev.*, 2021, **121**, 7346–7397; (*e*) J. Bae and E. J. Cho, *ACS Catal.*, 2023, **13**, 13540–13560.
5 (*a*) A. Bader and E. Lindner, *Coord. Chem. Rev.*, 1991, **108**, 27–110; (*b*) C. S. Slone, D. A. Weinberger and C. A. Mirkin, *Prog. Inorg. Chem.*, 1999, **48**, 233–350; (*c*) P. Braunstein and F. Naud, *Angew. Chem., Int. Ed.*, 2001, **40**, 680–699.
6 M. C. Gimeno, The chemistry of gold, in *Modern Supramolecular Gold Chemistry: Gold–Metal Interactions and Applications*, ed. A. Laguna, Wiley-VCH, Weinheim, Germany, 2009, pp. 1–63.
7 A. Zeineddine, L. Estévez, S. Mallet-Ladeira, K. Miqueu, A. Amgoune and D. Bourissou, *Nat. Commun.*, 2017, **8**, 565.
8 C. C. Chintawar, V. W. Bhoyare, M. V. Mane and N. T. Patil, *J. Am. Chem. Soc.*, 2022, **144**, 7089–7095.
9 (*a*) H. Grutzmacher, *Angew. Chem., Int. Ed.*, 2008, **47**, 1814–1818; (*b*) J. R. Khusnutdinova and D. Milstein, *Angew. Chem., Int. Ed.*, 2015, **54**, 12236–12273; (*c*) J. N. H. Reek, B. de Bruin, S. Pullen, T. J. Mooibroek, A. M. Kluwer and X. Caumes, *Chem. Rev.*, 2022, **122**, 12308–12369.
10 X. Cheng and L. Zhang, *CCS Chem.*, 2021, **3**, 1989–2002.
11 Y. Wang, Z. Wang, Y. Li, G. Wu, Z. Cao and L. Zhang, *Nat. Commun.*, 2014, **5**, 3470.
12 Z. Wang, C. Nicolini, C. Hervieu, Y.-F. Wong, G. Zanoni and L. Zhang, *J. Am. Chem. Soc.*, 2017, **139**, 16064–16067.
13 (*a*) R. C. J. Atkinson, V. C. Gibson and N. J. Long, *Chem. Soc. Rev.*, 2004, **33**, 313–328; (*b*) R. Gómez Arrayás, J. Adrio and J. C. Carretero, *Angew. Chem., Int. Ed.*, 2006, **45**, 7674–7715; (*c*) L. Cunningham, A. Benson and P. J. Guiry, *Org. Biomol. Chem.*, 2020, **18**, 9329–9370; (*d*) P. Štěpnička, *Dalton Trans.*, 2022, **51**, 8085–8102.
14 (*a*) O. Bárta, R. Gyepes, I. Císařová, A. Alemayehu and P. Štěpnička, *Dalton Trans.*, 2020, **49**, 4225–4229; (*b*) O. Bárta, I. Císařová and P. Štěpnička, *Dalton Trans.*, 2021, **50**, 14662–14671; (*c*) V. Varmužová, F. Horký and P. Štěpnička, *New J. Chem.*, 2021, **45**, 3319–3327; (*d*) M. Navrátil, I. Císařová and P. Štěpnička, *Dalton Trans.*, 2022, **51**, 14618–14629; (*e*) Z. Leitner, I. Císařová and P. Štěpnička, *New J. Chem.*, 2023, **47**, 5930–5938; (*f*) M. Navrátil, I. Císařová and P. Štěpnička, *J. Organomet. Chem.*, 2023, **983**, 122573; (*g*) F. Horký, M. Neubrand, I. Císařová, J. Schulz and P. Štěpnička, *ChemPlusChem*, 2023, **88**, e202300196; (*h*) C. Binnani, Z. Leitner, I. Císařová and P. Štěpnička, *Eur. J. Inorg. Chem.*, 2024, **27**, e202300644.
15 M. Stradiotto, R. Lundgren and K. Hesp, *Synlett*, 2011, 2443–2458.
16 K. Škoch, I. Císařová, J. Schulz, U. Siemeling and P. Štěpnička, *Dalton Trans.*, 2017, **46**, 10339–10354.
17 J. M. Brunel, B. Faure and M. Maffei, *Coord. Chem. Rev.*, 1998, **178–180**, 665–698.
18 P. Štěpnička, B. Schneiderová, J. Schulz and I. Císařová, *Organometallics*, 2013, **32**, 5754–5765 and ref. 16.
19 S. I. Kirin, H.-B. Kraatz and N. Metzler-Nolte, *Chem. Soc. Rev.*, 2006, **35**, 348–354.
20 J. A. Adeleke and L.-K. Liu, *Acta Crystallogr., Sect. C: Cryst. Struct. Commun.*, 1993, **49**, 680–682.
21 M. J. Verschoor-Kirss, O. Hendricks, C. M. Verschoor, R. Conry and R. U. Kirss, *Inorg. Chim. Acta*, 2016, **450**, 30–38.
22 C. Sambiagio, S. P. Marsden, A. J. Blacker and P. C. McGowan, *Chem. Soc. Rev.*, 2014, **43**, 3525–3550.
23 (*a*) J. F. Hartwig, *Angew. Chem., Int. Ed.*, 1998, **37**, 2046–2067; (*b*) J. P. Wolfe, S. Wagaw, J.-F. Marcoux and S. L. Buchwald, *Acc. Chem. Res.*, 1998, **31**, 805–818; (*c*) B. H. Yang and S. L. Buchwald, *J. Organomet. Chem.*, 1999, **576**, 125–146; (*d*) D. S. Surry and S. L. Buchwald, *Chem. Sci.*, 2011, **2**, 27–50; (*e*) R. J. Lundgren and M. Stradiotto, *Chem. – Eur. J.*, 2012, **18**, 9758–9769; (*f*) M. M. Heravi, Z. Kheilkordi, V. Zadsirjan, M. Haydari and M. Malmir, *J. Organomet. Chem.*, 2018, **861**, 17–104; (*g*) R. Dorel, C. P. Grugel and A. Haydl, *Angew. Chem., Int. Ed.*, 2019, **58**, 17118–17129.
24 M. Corpet and C. Gosmini, *Synthesis*, 2014, 2258–2271.
25 A. M. Berman and J. S. Johnson, *J. Am. Chem. Soc.*, 2004, **126**, 5680–5681.

26 I. R. Butler and R. L. Davies, *Synthesis*, 1996, 1350–1354.
27 (*a*) A. Zirakzadeh, A. Herlein, M. A. Gross, K. Mereiter, Y. Wang and W. Weissensteiner, *Organometallics*, 2015, **34**, 3820–3832; (*b*) K. Sünkel and S. Bernhartzeder, *J. Organomet. Chem.*, 2011, **696**, 1536–1540.
28 S. Dey, F. Roesler, C. Bruhn, Z. Kelemen and R. Pietschnig, *Inorg. Chem. Front.*, 2023, **10**, 3828–3843.
29 C. Metallinos, J. Zaifman, L. Belle, L. Dodge and M. Pilkington, *Organometallics*, 2009, **28**, 4534–4543.
30 (*a*) O. Bárta, I. Císařová, J. Schulz and P. Štěpnička, *New J. Chem.*, 2019, **43**, 11258–11262; (*b*) J. Schulz, P. Vosáhlo, F. Uhlík, I. Císařová and P. Štěpnička, *Organometallics*, 2017, **36**, 1828–1841.
31 K. Heinze and M. Schlenker, *Eur. J. Inorg. Chem.*, 2004, 2974–2988.
32 (*a*) A. Appel, F. Jäkle, T. Priermeier, R. Schmid and M. Wagner, *Organometallics*, 1996, **15**, 1188–1194; (*b*) M. Scheibitz, M. Bolte, J. W. Bats, H.-W. Lerner, I. Nowik, R. H. Herber, A. Krapp, M. Lein, M. C. Holthausen and M. Wagner, *Chem. – Eur. J.*, 2005, **11**, 584–603.
33 (*a*) G. Knizia, *J. Chem. Theory Comput.*, 2013, **9**, 4834–4843; (*b*) G. Knizia and J. E. M. N. Klein, *Angew. Chem., Int. Ed.*, 2015, **54**, 5518–5522.
34 (*a*) J. E. M. N. Klein, B. Miehlich, M. S. Holzwarth, M. Bauer, M. Milek, M. M. Khusniyarov, G. Knizia, H.-J. Werner and B. Plietker, *Angew. Chem., Int. Ed.*, 2014, **53**, 1790–1794; (*b*) L. Nunes dos Santos Comprido, J. E. M. N. Klein, G. Knizia, J. Kästner and A. S. K. Hashmi, *Angew. Chem., Int. Ed.*, 2015, **54**, 10336–10340; (*c*) F. F. Mulks, A. S. K. Hashmi and S. Faraji, *Organometallics*, 2020, **39**, 1814–1823; (*d*) L. Nunes dos Santos Comprido, J. E. M. N. Klein, G. Knizia, J. Kästner and A. S. K. Hashmi, *Chem. – Eur. J.*, 2016, **22**, 2892–2895; (*e*) D. Sorbelli, L. Nunes dos Santos Comprido, G. Knizia, A. S. K. Hashmi, L. Belpassi, P. Belanzoni and J. E. M. N. Klein, *ChemPhysChem*, 2019, **20**, 1671–1679; (*f*) H. Braunschweig, R. D. Dewhurst, J. O. C. Jiménez-Halla, E. Matito and J. H. Muessig, *Angew. Chem., Int. Ed.*, 2018, **57**, 412–416; (*g*) I. F. Leach and J. E. M. N. Klein, *ACS Cent. Sci.*, 2024, **10**, 1406–1414.
35 (*a*) I. Mayer, *Chem. Phys. Lett.*, 1983, **97**, 270–274; (*b*) I. Mayer, *Theor. Chim. Acta*, 1985, **67**, 315–322.
36 D. Cremer and J. A. Pople, *J. Am. Chem. Soc.*, 1975, **97**, 1354–1358.
37 (*a*) F. Canales, M. C. Gimeno, P. G. Jones, A. Laguna and M. D. Villacampa, *Dalton Trans.*, 2005, 3005–3015; (*b*) T. A. Fernandes, H. Solařová, I. Císařová, F. Uhlík, M. Štícha and P. Štěpnička, *Dalton Trans.*, 2015, **44**, 3092–3108 and ref. 31, 38 and 42.
38 K. Rössler, T. Rüffer, B. Walfort, R. Packheiser, R. Holze, M. Zharnikov and H. Lang, *J. Organomet. Chem.*, 2007, **692**, 1530–1545.
39 R. M. Gomila and A. Frontera, *Dalton Trans.*, 2025, **54**, 3095–3105.
40 A. S. K. Hashmi, J. P. Weyrauch, W. Frey and J. W. Bats, *Org. Lett.*, 2004, **6**, 4391–4394.
41 J. Schulz, J. Antala, D. Rezazgui, I. Císařová and P. Štěpnička, *Inorg. Chem.*, 2023, **62**, 14028–14043.
42 Z. Lu, G. B. Hammond and B. Xu, *Acc. Chem. Res.*, 2019, **52**, 1275–1288.
43 P. Vosáhlo and P. Štěpnička, *New J. Chem.*, 2023, **47**, 4510–4520.
44 (*a*) P. G. Jones and A. F. Williams, *J. Chem. Soc., Dalton Trans.*, 1977, 1430–1434; (*b*) P. G. Jones and A. G. Maddock, *J. Chem. Soc., Dalton Trans.*, 1977, 1434–1439.
45 (*a*) D. Weber and M. R. Gagné, *Org. Lett.*, 2009, **11**, 4962–4965; (*b*) S. G. Weber, F. Rominger and B. F. Straub, *Eur. J. Inorg. Chem.*, 2012, 2863–2867.
46 Z. Zheng, X. Ma, X. Cheng, K. Zhao, K. Gutman, T. Li and L. Zhang, *Chem. Rev.*, 2021, **121**, 8979–9038.
47 W. He, C. Li and L. Zhang, *J. Am. Chem. Soc.*, 2011, **133**, 8482–8485.
48 (*a*) Y. Luo, K. Ji, Y. Li and L. Zhang, *J. Am. Chem. Soc.*, 2012, **134**, 17412–17415; (*b*) K. Ji, Y. Zhao and L. Zhang, *Angew. Chem., Int. Ed.*, 2013, **52**, 6508–6512.
49 (*a*) CCDC 2517190: Experimental Crystal Structure Determination, 2026, DOI: 10.5517/ccdc.csd.cc2qhbp8; (*b*) CCDC 2517191: Experimental Crystal Structure Determination, 2026, DOI: 10.5517/ccdc.csd.cc2qhbq9; (*c*) CCDC 2517192: Experimental Crystal Structure Determination, 2026, DOI: 10.5517/ccdc.csd.cc2qhbrb; (*d*) CCDC 2517193: Experimental Crystal Structure Determination, 2026, DOI: 10.5517/ccdc.csd.cc2qhbsc; (*e*) CCDC 2517194: Experimental Crystal Structure Determination, 2026, DOI: 10.5517/ccdc.csd.cc2qhbtd; (*f*) CCDC 2517195: Experimental Crystal Structure Determination, 2026, DOI: 10.5517/ccdc.csd.cc2qhbvf; (*g*) CCDC 2517196: Experimental Crystal Structure Determination, 2026, DOI: 10.5517/ccdc.csd.cc2qhbwg; (*h*) CCDC 2517197: Experimental Crystal Structure Determination, 2026, DOI: 10.5517/ccdc.csd.cc2qhbxh; (*i*) CCDC 2517198: Experimental Crystal Structure Determination, 2026, DOI: 10.5517/ccdc.csd.cc2qhbyj; (*j*) CCDC 2517199: Experimental Crystal Structure Determination, 2026, DOI: 10.5517/ccdc.csd.cc2qhbzk; (*k*) CCDC 2517200: Experimental Crystal Structure Determination, 2026, DOI: 10.5517/ccdc.csd.cc2qhc0m; (*l*) CCDC 2517201: Experimental Crystal Structure Determination, 2026, DOI: 10.5517/ccdc.csd.cc2qhc1n; (*m*) CCDC 2517202: Experimental Crystal Structure Determination, 2026, DOI: 10.5517/ccdc.csd.cc2qhc2p; (*n*) CCDC 2517203: Experimental Crystal Structure Determination, 2026, DOI: 10.5517/ccdc.csd.cc2qhc3q; (*o*) CCDC 2517204: Experimental Crystal Structure Determination, 2026, DOI: 10.5517/ccdc.csd.cc2qhc4r; (*p*) CCDC 2517205: Experimental Crystal Structure Determination, 2026, DOI: 10.5517/ccdc.csd.cc2qhc5s; (*q*) CCDC 2517206: Experimental Crystal Structure Determination, 2026, DOI: 10.5517/ccdc.csd.cc2qhc6t; (*r*) CCDC 2517207: Experimental Crystal Structure

Determination, 2026, DOI: 10.5517/ccdc.csd.cc2qhc7v; (*s*) CCDC 2517208: Experimental Crystal Structure Determination, 2026, DOI: 10.5517/ccdc.csd.cc2qhc8w; (*t*) CCDC 2517209: Experimental Crystal Structure Determination, 2026, DOI: 10.5517/ccdc.csd.cc2qhc9x; (*u*) CCDC 2517210: Experimental Crystal Structure Determination, 2026, DOI: 10.5517/ccdc.csd.cc2qhcby; (*v*) CCDC 2517404: Experimental Crystal Structure Determination, 2026, DOI: 10.5517/ccdc.csd.cc2qhkld; (*w*) CCDC 2522540: Experimental Crystal Structure Determination, 2026, DOI: 10.5517/ccdc.csd.cc2qnx8l.